Cite this: *Nanoscale*, 2011, **3**, 1675

www.rsc.org/nanoscale

PAPER

A catalyst-free and facile route to periodically ordered and *c*-axis aligned ZnO nanorod arrays on diverse substrates†

Daragh Byrne, Enda McGlynn,* Joseph Cullen and Martin O. Henry

Received 29th November 2010, Accepted 24th December 2010
DOI: 10.1039/c0nr00919a

In this work we present a method for the deposition of periodically ordered, *c*-axis aligned ZnO nanorod arrays. By using chemical bath deposited films in conjunction with silica templating through nanosphere monolayers, masks suitable for high temperature deposition are created. A vapour phase transport technique is then used to deposit ordered arrays, quickly and inexpensively in a manner ideal for low cost, scalable and reproducible growth on a diverse range of substrates.

Introduction

ZnO nanostructures are of considerable interest due to their favorable properties for many potential device applications. Being a relatively inexpensive wide band gap II–VI semiconductor with a direct transition of 3.3 eV at room temperature,[1] ZnO can be considered an excellent candidate for optoelectronic,[2,3] photovoltaic,[4] gas sensing,[5] catalytic,[6] micro-energy generation,[7] field emission[8] and many other applications. Many of these applications are enhanced when the ZnO is deposited as nanorods vertically aligned with respect to the substrate, where the high surface area and/or surface effects contribute to the device performance.[4,7,9,10] Consequently there have been numerous reports detailing aligned nanorod growth techniques such as chemical bath deposition (CBD),[11] electro-deposition,[12] vapour phase transport (VPT),[13–15] solid phase deposition[16] and chemical vapour deposition.[17] More recently, it has been demonstrated that CBD growth techniques can be combined with high temperature VPT growth to deposit highly aligned ZnO nanorods.[18–20] This approach has the advantage of producing nanorods of excellent quality and a high degree of vertical alignment on a wide variety of substrates (including non-epitaxially matched ones). Additionally, for certain applications such as field emission and optoelectronic applications, not only is it important to have nanorods of high quality and alignment, it is also necessary to control the nanorod density and/or position.[8,15] Control of this nature has previously been demonstrated for ZnO and other materials, using approaches such as nanosphere lithography (NSL), laser interference lithography and carbonised photoresist lithography.[8,21–27] Significant progress has been made in depositing ordered arrays by low temperature techniques such as CBD in combination with photoresists,[26,27] but higher temperature techniques such as VPT represent a greater challenge due to the high processing temperatures necessary for the deposition of high crystalline and optical quality ordered arrays and their incompatibility with photoresist materials. Consequently many of the reports dealing with ordered and aligned high temperature deposited arrays use selective positioning of catalysts such as gold to control the nanorod positioning,[8,22–24,28,29] while relying on epitaxial matching between the substrate and the deposited material to achieve nanorod alignment. This limits the choice of substrates to those that have sufficiently close epitaxial matching to achieve alignment, while the presence of a catalyst can lead to both nanowire contamination as well as changes in morphology which can be detrimental for applications such as field emission where sharp facet edges may be crucial to performance.[30]

In this work we report a high temperature growth technique using nanosphere lithography which does not rely on either epitaxially matched substrates or the use of catalysts. This distinct advantage over catalytic methods means that the only limitation on the choice of substrate is the processing temperature, while the potential for catalyst contamination is negated. Previously our group and others have reported methods, combining CBD with VPT, which produce very high quality aligned nanorods. We show here that these methods, in combination with a modified NSL technique,[31] serve as an ideal platform for depositing ordered periodic arrays of aligned ZnO

School of Physical Sciences, National Centre for Plasma Science and Technology, Dublin City University, Glasnevin, Dublin 9, Ireland. E-mail: enda.mcglynn@dcu.ie; Fax: +353 (0)1 7005384; Tel: +353 (0)1 7005387

† Electronic supplementary information (ESI) available: SEM image of thin ZnO films deposited by CBD from (a) direct decomposition of zinc acetate at 65 °C and zinc nitrate with HMT. Schematic representation of the effects of poor surface contact between the nanosphere monolayer and the CBD ZnO buffer layer on the VPT deposition. Schematic representation and SEM image of the effects of surface roughness on contact between the underlying CBD layer and the nanospheres and its effect on the silica template. SEM image of a silica template showing voids, domain boundaries and bi-layer created from trapped nanospheres. SEM images showing 90° views of a ZnO ordered array where additional long and thin, high aspect ratio nanorods and dual nanorod nucleation/crystal twinning was observed. SEM images of 1 μm spaced VPT grown ordered arrays on *a*-sapphire and quartz substrates. PL of an ordered nanorod array over a broad spectral range showing evidence of the structured green band. See DOI: 10.1039/c0nr00919a

nanorods. We call this method catalyst-free inverse nanosphere lithography (CF-INSL). This method is both easily implemented and produces ordered arrays of well aligned nanorods with excellent optical quality. In addition, the technique is low cost and fully suitable for non-epitaxially matched substrates.

Experimental

Step 1: ZnO buffer layer

Silicon substrates with (111) orientation and a native oxide layer were coated with a ZnO seed layer by drop coating a 5 mM solution of zinc acetate in absolute ethanol.[32] 4 μl of zinc acetate solution per cm^2 of silicon was applied to the substrate surface for 20 seconds before being rinsed with absolute ethanol and dried with a nitrogen stream. This process was repeated 4–5 times after which the substrates were annealed at 350 °C for 30 minutes to yield a thin ZnO seed layer. The seed layers were grown into a thicker ZnO buffer layer, by submerging them in a 25 mM zinc acetate in DI-H_2O solution at 60–70 °C for two hours. The ZnO buffer layers were cleaned by sonication in fresh DI-H_2O and dried under a nitrogen stream.

Step 2: silica mask

The ZnO buffer layers were first coated with an ordered array of polystyrene nanospheres by a method reported elsewhere.[33,34] To improve adhesion and contact between the buffer layers and the spheres, the samples were mounted vertically on a spin coater with the nanosphere coating facing the axis of rotation and spun at 2000 rpm for 30 seconds, followed by annealing at 110 °C for 40 seconds. A silica sol was prepared by mixing 1 ml of TEOS with 1 ml of 0.1 M HCl in 20 ml of absolute ethanol for three hours. Immediately before use this solution was diluted with an equal volume of ethanol. Each sample was then drop coated with 20 μl of sol, which was allowed to evaporate for a short period before the excess was removed by spinning at 2500 rpm for 30 seconds. The silica masks were further dried for 10 minutes by heating at 90 °C. The polystyrene spheres were removed by dissolution in toluene, then in acetone. Finally the silica template was densified, by heating at 510 °C at a temperature ramp rate of 20 °C min^{-1} and held at the final temperature for 15 minutes.

Step 3: VPT deposition and sample characterisation

Equal masses of graphite and ZnO (0.06 g) were thoroughly mixed and transferred into an alumina boat. The substrates were placed over the mixture with the seeded/templated side facing the graphite/ZnO powder. The boat was heated at 900 °C in the centre of a single zone horizontal tube furnace, with a 90 sccm flow of argon for 1 hour, before being allowed to cool to room temperature.

The morphologies and crystal structures of the deposits were examined using SEM (Karl-Zeiss EVO series) and XRD (Bruker AXS D8 Advance Texture Diffractometer). The photoluminescence spectra were acquired using the 325 nm line of He–Cd laser with a Bomem, Hartmann & Braun DA8 FT spectrometer with the samples in a closed cycle cryostat (Janis Research Co. Inc.).

Results and discussion

The CF-INSL deposition method is composed of three facile steps, the first of which is to deposit a thin ZnO buffer layer on the substrate. This provides both the nucleation sites and alignment necessary for later steps. Once deposited, the second step is to cap this thin buffer layer with an ordered silica nanohole template. This nanohole template provides the positional control during the final stage of the process, a high temperature VPT deposition. The alignment of the underlying ZnO film ensures that any nanorod growth that takes place during the VPT stage is also aligned with respect to the substrate, while the silica template ensures that the nanorods only grow in the locations where the nanospheres were in contact with the CBD deposited film. We now consider each of the three steps in more detail.

ZnO buffer layer

The first step of this process involves the deposition of a ZnO film by a chemical bath method. Frequently, the decomposition of HMT in solutions of zinc salts has been used to deposit high quality aligned ZnO nanostructures. For reasons that will be discussed in more detail later, this method was less suitable for our process. Instead ZnO films were grown by submerging the seeded substrates in a 25 mM solution of zinc acetate at ~65 °C for various reaction times, without the addition of any sources of hydroxide or amine species. While CBD deposition is synonymous with the growth of nanorods, by extending the deposition times and in the absence of any lateral facet capping agents, the nanorods form a near continuous columnar film with little or no inter-column spaces evident. Examples of such films grown from varying reaction precursors are shown in the (ESI†) (Fig. S1). In both cases shown in Fig. S1†, a thin dense columnar film is deposited, which is suitable for the deposition of aligned nanowires by VPT. For reasons discussed later it was found that the zinc acetate precursor yielded better results for ordered array VPT deposition.

The continuous films deposited directly from decomposing zinc acetate are well textured with respect to the substrate as demonstrated by XRD analysis shown in Fig. 1(a)(iii) and (b)(vi). Only peaks ascribed to the ZnO (002) (~34.4°) plane and silicon (111) and (222) (~28.4° and ~59°) planes were detected. Rocking curve analysis of the ZnO (002) peak at 34.4° suggests that the as-deposited films are well textured with respect to the surface normal with a FWHM of ~9.8°. While there are many reports of high quality aligned ZnO films/nanostructures grown by CBD or hydrothermal methods, few report the rocking curve FWHM for polycrystalline films on non-epitaxially matched substrates, making a direct comparison difficult. However, a FWHM of ~9.8° is in broad agreement with results published by Wang *et al.* and Yang *et al.*[35,36] The remaining XRD data in Fig. 1(a and b) are discussed later.

Silica template

We consider now the necessary conditions for formation of suitable silica templates in the second step of the CF-INSL process. To achieve a large uniform silica template, coating the self-assembled nanosphere monolayer onto the CBD buffer layer is a critical step. For this work we used a self-assembly on the surface of water technique reported by Rybczynski *et al.*[33,34] By

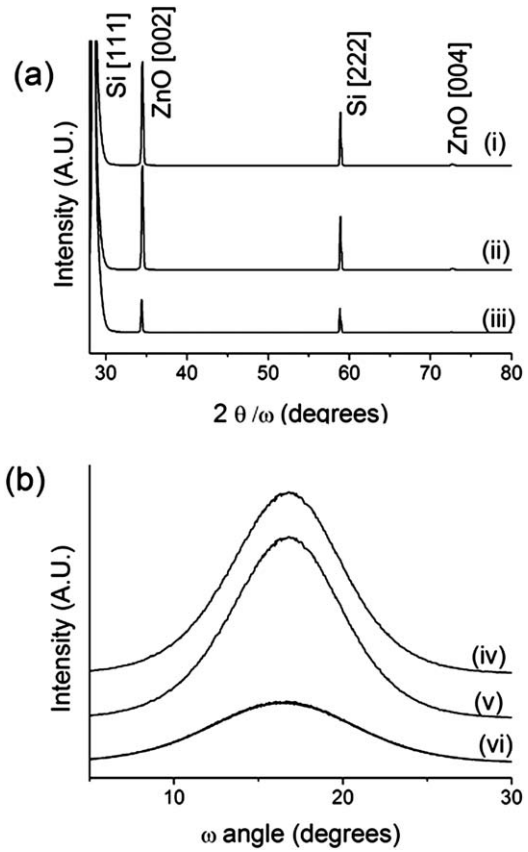

Fig. 1 XRD $2\theta/\omega$ scan of (a) (i) VPT grown patterned array on CBD buffer layer, (ii) VPT grown patterned array on two CBD growths buffer layer and (iii) ZnO buffer layer derived from zinc acetate. XRD rocking curve of the ZnO (002) peak for (b) (iv) VPT grown patterned array on CBD buffer layer, (v) VPT grown patterned array on two CBD growths buffer layer and (vi) ZnO buffer layer derived from zinc acetate.

carefully lifting the substrate through a colloidal crystal assembled on the surface of water, the nanosphere monolayer can be transferred to the substrate/CBD surface. For clean flat substrates such as Si wafers, the monolayers appear to make good contact with the substrate. For catalytic approaches, where gold is to be deposited through the apertures created by the spheres, it is in any case debatable if the degree of contact between the spheres and the substrate is a significant factor. For silica templating, however, it is essential that the spheres are in good contact with the underlying ZnO, so as to prevent the silica sol seeping under the spheres and completely masking the CBD buffer layer. This problem is compounded by variations in the buffer layer thickness deposited by CBD. This can lead to patchy growth during the VPT stage, a schematic and an example of which are shown in the ESI† (Fig. S2). Difficulties with the contact between buffer layer and spheres can be partially offset by using centripetal force to drive the spheres close to the ZnO buffer layer without significantly disturbing the HCP pattern. This is achieved by spinning the sample at ~2000 rpm with the nanosphere coated surface facing the axis of rotation. The substrate is then annealed gently to improve the adhesion of the polystyrene nanosphere monolayer.

The surface roughness of the buffer layer also plays a key role during templating. As seen in the ESI† (Fig. S3), another problem can arise if the surface of the buffer layer is excessively rough, whereby the nanospheres may not contact the buffer layer at just one location along the central axis of the sphere perpendicular to the substrate. Post-silica deposition, this roughness may lead to multiple VPT nucleation sites being formed per sphere, distorting the HCP pattern. This lies behind the choice of zinc acetate for the deposition of the buffer layer. Despite the reduced quality of the ZnO deposited as compared to other CBD techniques, empirical results suggest that the films formed by zinc acetate at low temperatures, *i.e.* at a slow rate of deposition, tend to be smoother than those formed by the faster decomposition of HMT methods. While it is unclear why this is the case, we speculate that the reduced growth rate allows for a more thorough mixing of the reaction solution leading to more uniform deposition. By reducing the surface roughness, we have found that the nanospheres make better contact with the ZnO buffer layer leading to a reduction in the number of faults in the silica template.

The choice of catalyst used to form the silica sol from TEOS was also examined to see if this had any impact on the process. Despite the sensitivity of ZnO to acids, sols prepared from HCl or H_2SO_4 were found to perform better than those prepared from NaOH. The templates prepared in this manner show a high degree of uniformity, a typical example of which is shown in Fig. 2. While defects are visible in many HCP patterns (see regions indicated by arrows in Fig. S4 in the ESI†), it is clear in all cases that these defects are the result of imperfections in the nanosphere monolayer dispersed on the surface of the water. These defects include domain boundaries, voids and bi-layers caused by rogue nanospheres trapped under the monolayer.

VPT deposition

Two strategies for the final deposition of the ordered nanorod array were examined. Firstly, nanorods were grown by VPT using a method reported in more detail elsewhere,[19,20] directly through the silica template. The second method involved a second zinc acetate chemical bath deposition to initiate ordered nanorod growth, followed by VPT to deposit the ordered nanorod array. The success of this direct VPT deposition process

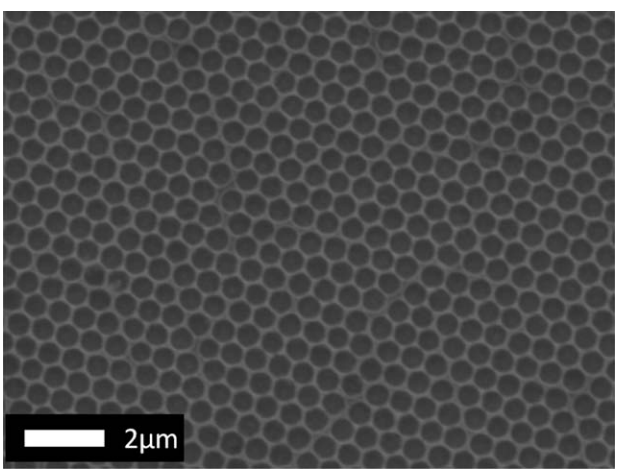

Fig. 2 SEM images of a typical silica template deposited on top of a CBD ZnO buffer layer.

through the silica mask for producing ordered well aligned nanorod arrays is evident in Fig. 3.

Two nanosphere sizes, 1 μm and 500 nm, were tested and in both cases the nanorods deposited were predominantly confined to the locations where the nanospheres were in contact with the underlying CBD buffer layer. When 500 nm spheres were used, the majority of nanorods were 2.5–3 μm in length with a diameter of 140–170 nm. When 1 μm spheres were used the average length reduced to 1.5–2 μm with diameters 200–260 nm. Interestingly, this represented a reduction in aspect ratio approximately inversely equal to the reduction in sphere size, which suggests that the pore size in the silica template not only influences the nanorod position but also its morphology, which has been observed previously.[27] In both sample sets, two additional nanorod morphologies were observed, examples of which are shown in the ESI† (Fig. S5). The first additional morphology consisted of nanorods with substantially higher aspect ratios; typically these rods had lengths ranging from 3 μm to 15 μm with diameters centred around 100 nm. They have been observed to nucleate from the tips of shorter nanorods,

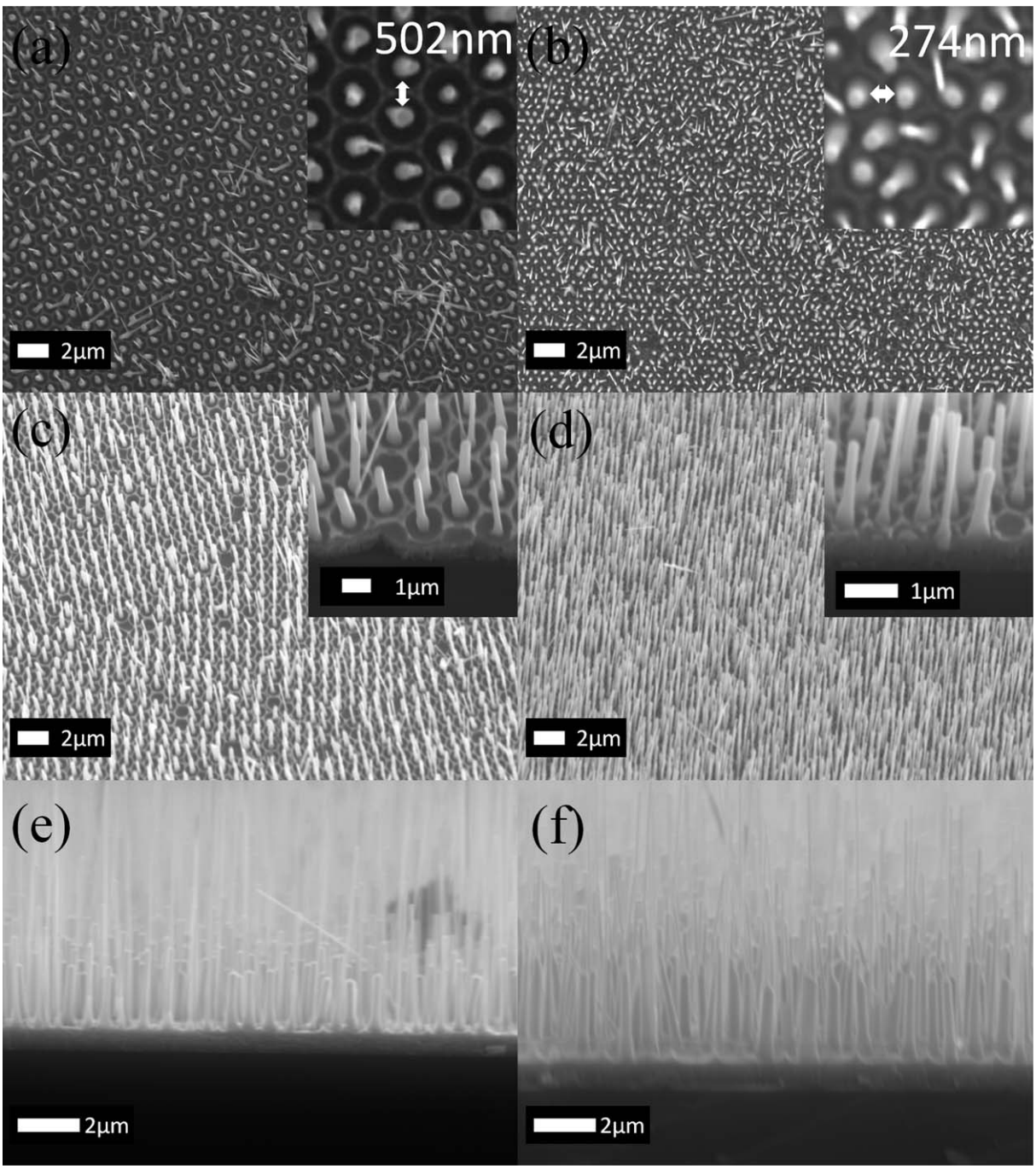

Fig. 3 SEM images of a 1 μm spaced VPT grown ordered array in plan view (a), 45° view (b) and 90° view (c). Parts (d) to (f) show the corresponding views for a 500 nm spaced array.

from the holes in the silica template in conjunction with a "regular" sized nanorod and from small cracks that have developed in the silica template during the growth process. The second morphology consists of two nanorods nucleating from the same location and apparently sharing the same base. Often these twinned crystals have an angle of approximately 60° between them. In both cases it is difficult to ascertain the precise origin or cause of these variations. Previously it has been reported that the ZnO buffer layers play a very important role during VPT deposition of non-templated ZnO nanorods.[37] For non-templated substrates nanorod nucleation takes place on the buffer layer at sites that are favorable by virtue of their orientation, morphology, energetics or crystalline quality. For templated substrates, the choice of nucleation site is severely constrained by the presence of the silica mask, forcing nucleation to take place at specific points irrespective of the underlying morphology of the buffer layer. As seen in Fig. S1†, despite care being taken in the preparation of the buffer layer, grain boundaries, cracks and surface roughness will still be present. We therefore believe that these underlying defects contribute significantly to the origin of the additional morphologies observed.

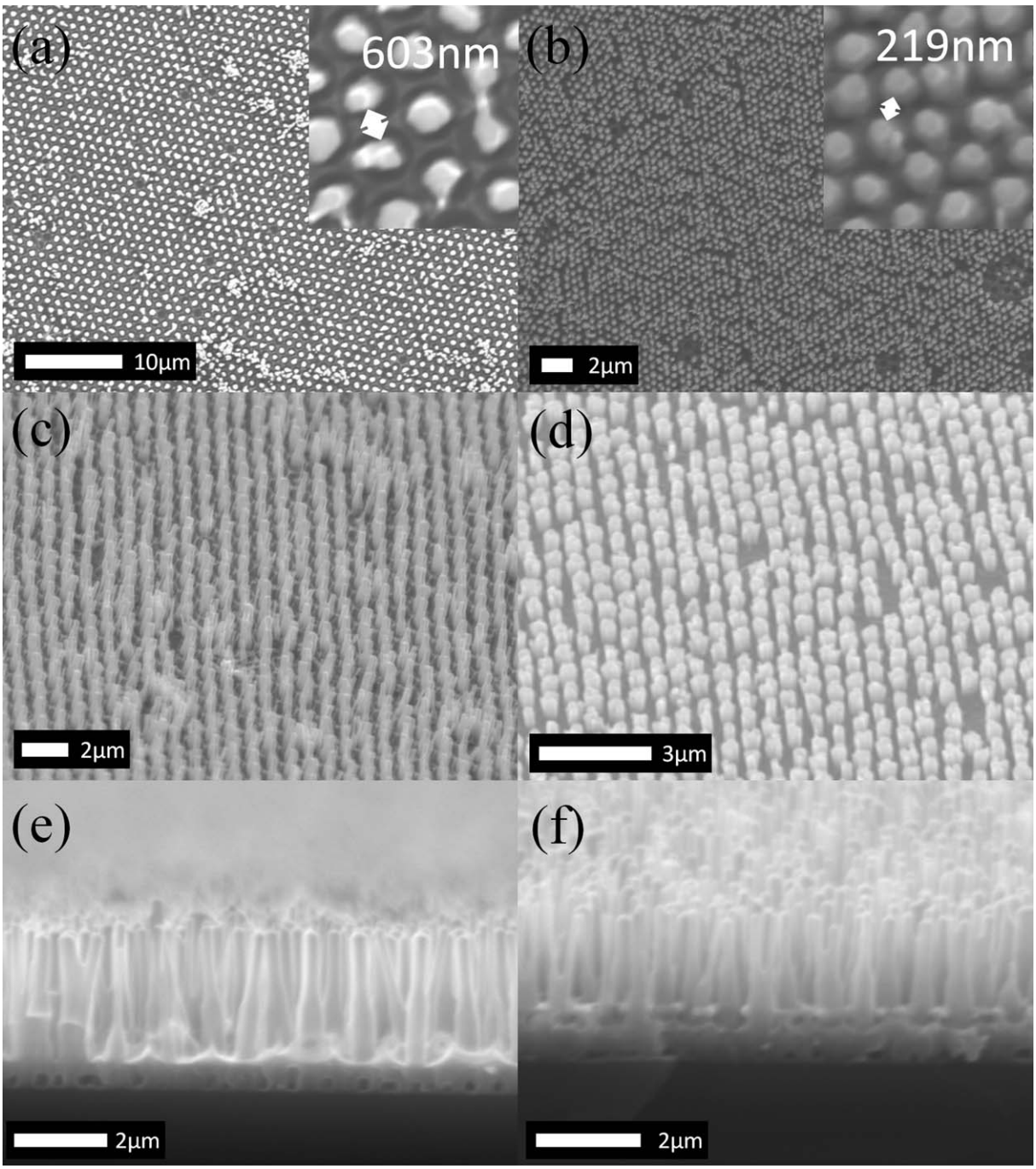

Fig. 4 SEM images of a 1 μm spaced VPT grown ordered array, grown on a substrate where a second CBD step was performed to initiate the nanorod growth, in plan view (a), 45° view (b) and 90° view (c). Parts (d) to (f) show the corresponding views for a 500 nm spaced array.

We now describe the second method used for the final deposition of ordered arrays. In this case, a second short chemical bath deposition was performed, after the silica template was densified. This initiated nanorod aligned growth prior to the VPT step. As can be seen in Fig. 4, by performing a second CBD, in combination with a decrease in the VPT temperature ramp rate (to discourage secondary nucleation of thin rods on shorter rods), the long high aspect ratio nanorods, seen in the sample deposited directly through the silica template, were completely eliminated. In addition, there was less evidence of multiple rods per nucleation site and crystal twinning. While some twinning did occur, these rods merged at the approximate location where the tip of the nanorods deposited during the second CBD was located. This again strongly suggests that the additional morphologies observed were due to the surface of the acetate deposited ZnO rather than the VPT deposition process itself. Substrates templated with 1 μm nanospheres had average rod lengths of ~2.8 μm with a diameter of 300 nm to 500 nm. For samples templated with 500 nm nanospheres the average rod length reduced to 1.8 μm with a diameter in the range of 250–400 nm. The inverse relationship observed between the rod spacing and aspect ratio was not observed for the second method. This may be due to the second CBD step altering the VPT nucleation process, creating a more homogenously sized nucleation site between spheres of different sizes. While some variation is observed in the nanorod morphology, this method allows the nanorod spacing/density to be controlled while keeping the rod dimensions within the same order of magnitude.

XRD analysis of the ordered nanorod arrays, as shown above in Fig. 1(a)((i) and (ii)), is similar to those of the underlying buffer layers (Fig. 1(a)(iii)) with only the ZnO (002) and (004) peaks being detected, indicating a high degree of nanorod alignment normal to the substrate surface. The FWHM of the rocking curves for the ZnO (002) peak (Fig. 1(b)(iv) and (v)) is rather broad at ~7.5°, showing only minor improvements over the CBD buffer layer. This would indicate that the material deposited during the VPT steps does not display a significantly higher degree of texture than that of the buffer layer, as expected. This remains the case whether one or two CBD growth steps are used prior to the final VPT growth step. Use of more complex buffer layer deposition methods such as pulsed laser deposition (PLD) could improve the buffer layer texture and thus that of the nanostructures deposited thereon.[38,39]

Finally, we note that the CF-INSL growth method described in detail above and optimised in our work for growth on Si substrates with a native oxide also works for a range of other substrates such as quartz and *a*-plane sapphire as shown in the ESI† (Fig. S6). These data clearly demonstrate that CF-INSL is compatible with a diverse range of substrates (including crystalline and non-crystalline substrates) and the nature of the technique, not relying on epitaxial matching, suggests its wider potential versatility.

Optical quality

Evidence that the CF-INSL deposited nanorods are of excellent optical quality comes from the photoluminescence spectra, with strong emission and very narrow bound exciton linewidths at low temperature as shown in Fig. 5. A range of spectral features can be clearly resolved in the spectra from the various samples, the brightest of which include I_2/SX, I_6 and I_9 lines.[40] The I_6 line centred around 3.361 eV is common to all our samples grown by CF-INSL and its presence is ascribed to Al impurities.[40] The presence of Al is easily understood as the substrate and reaction mixture are contained within an alumina boat during the deposition process. The average FWHM of this peak is 0.49 meV indicating that the material is of high optical quality. The I_9 line is found in the majority of our CF-INSL grown samples and is ascribed to the presence of indium.[41] While the precise origin of the indium is uncertain, it is a common impurity found in ZnO and may originate in the source powder used in our VPT system or from cumulative equipment contamination from previous experiments including some involving indium doping. A strong emission around 3.367 eV is also detected in some samples, corresponding to the so-called surface exciton (SX) line, which is closely associated with surface adsorbed impurities on nanostructured ZnO, leading to a surface bound exciton recombination.[42] PL over a broader spectral range for all samples shows evidence of visible broadband emission due to defects, with varying intensities relative to the UV bandedge emission. However, the wide range of factors which influence the UV to visible intensity ratio in nanostructures makes judgement of optical quality based on this ratio unreliable, and we have concentrated mainly on the low temperature bound exciton linewidths as the main indicator of optical quality in our samples.[43] PL data over both the UV and visible spectral ranges are shown in the ESI† (Fig. S7) for one sample, and evidence is seen of the structured green band, normally attributed to Cu defects in ZnO.[44]

In order to determine the PL contribution from the underlying buffer layer, samples were prepared without the final VPT deposition. The PL spectra of these samples were measured before and after a thermal cycle identical to that of the final VPT deposition process. From this it was found that PL contribution from the underlying CBD buffer layer, as shown in Fig. 5(e), is extremely weak. After the thermal annealing cycle identical to the VPT growth process, some improvement in the buffer layer PL signal was observed as seen in Fig. 5(f), however, the signal intensity is approximately 100 times weaker than its VPT equivalent. Interestingly prior to the annealing step the only peak detected is a broad peak at ~3.368 eV. Post-annealing this peak has been replaced with a feature close to the I_9 peak energy, suggesting that the origin of the I_9 peak in the VPT grown samples may be due to the equipment contamination referred to previously.

Conclusions

We have demonstrated a general, low cost method (CF-INSL) to grow high quality *c*-axis aligned ZnO nanorods on non-epitaxially matched substrates while maintaining control over the nanorod density/inter-rod spacing. This process uses only simple equipment and techniques which can be easily adapted and is compatible with both chemical solution based and higher temperature VPT growth methods. XRD and PL investigations confirm that not only are the nanorods well aligned, but they are also of excellent optical quality, very suitable for optoelectronic applications.

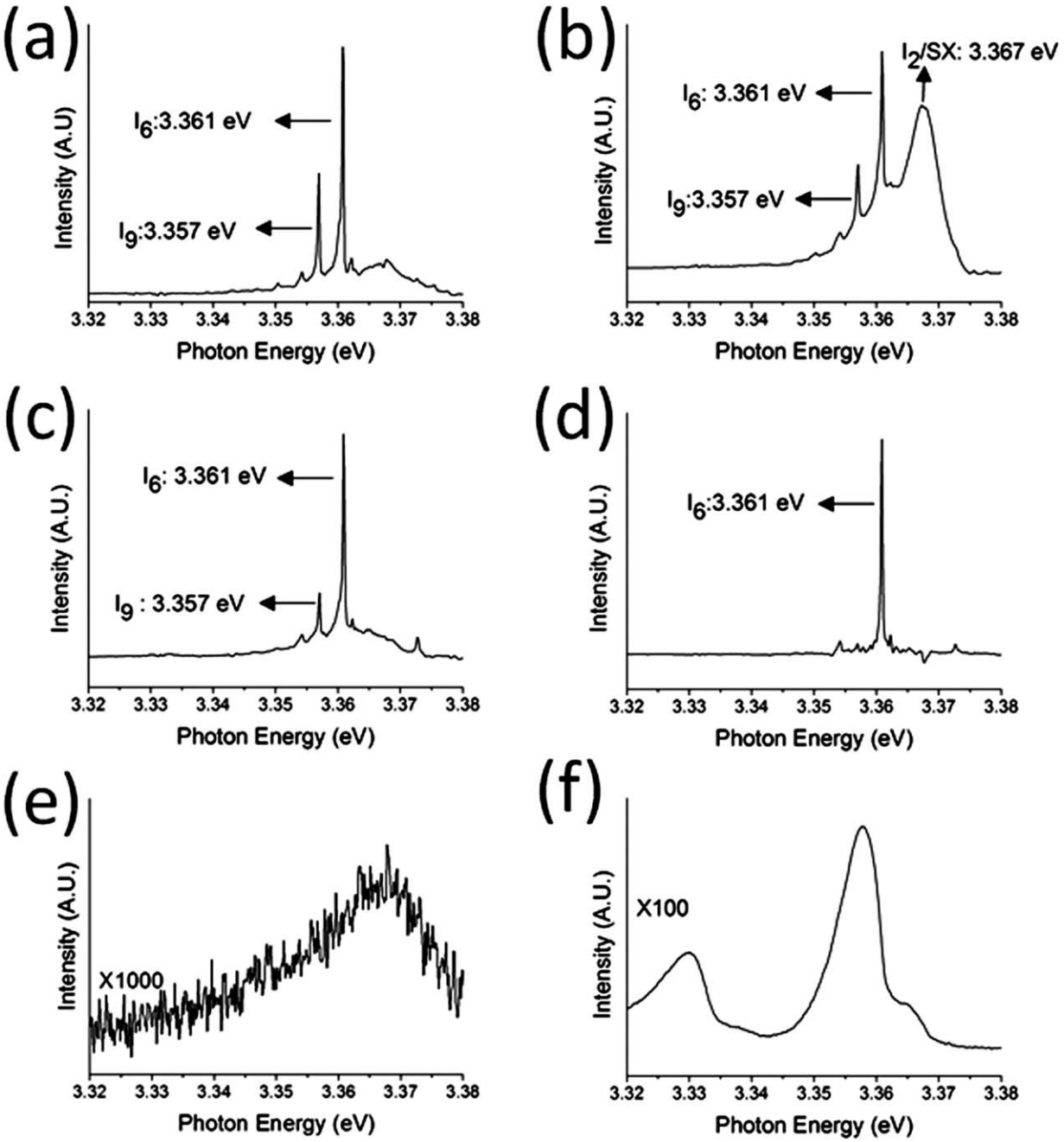

Fig. 5 Low temperature PL (~18 to 20 K) of: (a) VPT grown 1 μm patterned nanorod array corresponding to the sample shown in Fig. 3a; (b) 500 nm patterned array corresponding to Fig. 3b; (c) 1 μm patterned array corresponding to Fig. 4a; (d) 500 nm patterned array corresponding to Fig. 4b; (e) CBD buffer layer deposited from a zinc acetate solution; (f) CBD buffer layer deposited from a zinc acetate solution annealed using the same temperature profile as that used for the VPT deposition. All spectra were averaged over 2000 scans.

Acknowledgements

DB and EMCG acknowledge support from a Science Foundation Ireland Strategic Research Cluster grant entitled "Functional Oxides and Related Materials for Electronics" (FORME). DB and EMCG also gratefully acknowledge helpful discussions with Prof Martyn Pemble (Tyndall National Institute, Ireland—PI of FORME cluster). JC and MOH acknowledge support from Science Foundation Ireland under the Research Frontiers Programme (contract 08/RFP/PHY1558).

References

1 D. C. Reynolds, D. C. Look, B. Jogai, C. W. Litton, T. C. Collins, W. Harsch and G. Cantwell, *Phys. Rev. B: Condens. Matter*, 1998, **58**, 13276–13276.
2 X. X. WangWang, C. J. Summers and Z. L. Wang, *Nano Lett.*, 2004, **4**, 423–426.
3 M. H. Huang, S. Mao, H. Feick, H. Q. Yan, Y. Y. Wu, H. Kind, E. Weber, R. Russo and P. D. Yang, *Science*, 2001, **292**, 1897–1899.
4 M. Law, L. E. Greene, J. C. Johnson, R. Saykally and P. D. Yang, *Nat. Mater.*, 2005, **4**, 455–459.
5 H. Nanto, T. Minami and S. Takata, *J. Appl. Phys.*, 1986, **60**, 482–484.

6 N. Iwasa, S. Masuda, N. Ogawa and N. Takezawa, *Appl. Catal., A*, 1995, **125**, 145–157.
7 Z. L. Wang and J. H. Song, *Science*, 2006, **312**, 242–246.
8 D. F. Liu, Y. J. Xiang, X. C. Wu, Z. X. Zhang, L. F. Liu, L. Song, X. W. Zhao, S. D. Luo, W. J. Ma, J. Shen, W. Y. Zhou, G. Wang, C. Y. Wang and S. S. Xie, *Nano Lett.*, 2006, **6**, 2375–2378.
9 J. X. Wang, X. W. Sun, Y. Yang, H. Huang, Y. C. Lee, O. K. Tan and L. Vayssieres, *Nanotechnology*, 2006, **17**, 4995–4998.
10 C. J. Lee, T. J. Lee, S. C. Lyu, Y. Zhang, H. Ruh and H. J. Lee, *Appl. Phys. Lett.*, 2002, **81**, 3648–3650.
11 K. Govender, D. S. Boyle, P. B. Kenway and P. O'Brien, *J. Mater. Chem.*, 2004, **14**, 2575–2591.
12 M. J. Zheng, L. D. Zhang, G. H. Li and W. Z. Shen, *Chem. Phys. Lett.*, 2002, **363**, 123–128.
13 R. T. R. Kumar, E. McGlynn, M. Biswas, R. Saunders, G. Trolliard, B. Soulestin, J. R. Duclere, J. P. Mosnier and M. O. Henry, *J. Appl. Phys.*, 2008, **104**, 084309–084311.
14 J. Grabowska, K. K. Nanda, E. McGlynn, J. P. Mosnier and M. O. Henry, *Surf. Coat. Technol.*, 2005, **200**, 1093–1096.
15 R. T. R. Kumar, E. McGlynn, C. McLoughlin, S. Chakrabarti, R. C. Smith, J. D. Carey, J. P. Mosnier and M. O. Henry, *Nanotechnology*, 2007, **18**, 215704.
16 K. Huo, Y. Hu, J. Fu, X. Wang, P. K. Chu, Z. Hu and Y. Chen, *J. Phys. Chem. C*, 2007, **111**, 5876–5881.
17 P.-C. Chang, Z. Fan, D. Wang, W.-Y. Tseng, W.-A. Chiou, J. Hong and J. G. Lu, *Chem. Mater.*, 2004, **16**, 5133–5137.
18 D.-S. Kang, S. K. Han, J.-H. Kim, S. M. Yang, J. G. Kim, S.-K. Hong, D. Kim, H. Kim and J.-H. Song, *J. Vac. Sci. Technol., B: Microelectron. Nanometer Struct.–Process., Meas., Phenom.*, 2009, **27**, 1667–1672.
19 D. Byrne, E. McGlynn, M. O. Henry, K. Kumar and G. Hughes, *Thin Solid Films*, 2010, **518**, 4489–4492.
20 D. Byrne, E. McGlynn, K. Kumar, M. Biswas, M. O. Henry and G. Hughes, *Cryst. Growth Des.*, 2010, **10**, 2400–2408.
21 T. Y. Tsai, T. H. Chen, N. H. Tai, S. C. Chang, H. C. Hsu and T. J. Palathinkal, *Nanotechnology*, 2009, **20**, 305303.
22 D. F. Liu, Y. J. Xiang, Q. Liao, J. P. Zhang, X. C. Wu, Z. X. Zhang, L. F. Liu, W. J. Ma, J. Shen, W. Y. Zhou and S. S. Xie, *Nanotechnology*, 2007, **18**, 405303.
23 X. X. Zhang, D. F. Liu, L. H. Zhang, W. L. Li, M. Gao, W. J. Ma, Y. Ren, Q. S. Zeng, Z. Q. Niu, W. Y. Zhou and S. S. Xie, *J. Mater. Chem.*, 2009, **19**, 962–969.
24 H. J. Fan, B. Fuhrmann, R. Scholz, F. Syrowatka, A. Dadgar, A. Krost and M. Zacharias, *J. Cryst. Growth*, 2006, **287**, 34–38.
25 C. Cheng, M. Lei, L. Feng, T. L. Wong, K. M. Ho, K. K. Fung, M. M. T. Loy, D. Yu and N. Wang, *ACS Nano*, 2008, **3**, 53–58.
26 T.-U. Kim, J.-A. Kim, S. M. Pawar, J.-H. Moon and J. H. Kim, *Cryst. Growth Des.*, 2010, **10**, 4256–4261.
27 Y. Wei, W. Wu, R. Guo, D. Yuan, S. Das and Z. L. Wang, *Nano Lett.*, 2010, **10**, 3414–3419.
28 C. W. Yu, S. H. Lai, T. Y. Wang, M. D. Lan and M. S. Ho, *J. Nanosci. Nanotechnol.*, 2008, **8**, 4377–4381.
29 H. Zhou, J. Fallert, J. Sartor, R. J. B. Dietz, C. Klingshirn, H. Kalt, D. Weissenberger, D. Gerthsen, H. Zeng and W. Cai, *Appl. Phys. Lett.*, 2008, **92**, 132112–132113.
30 C. Li, G. J. Fang, L. Y. Yuan, N. S. Liu, J. Li, D. J. Li and X. Z. Zhao, *Appl. Surf. Sci.*, 2007, **253**, 8478–8482.
31 C. Li, G. S. Hong, P. W. Wang, D. P. Yu and L. M. Qi, *Chem. Mater.*, 2009, **21**, 891–897.
32 L. E. Greene, M. Law, D. H. Tan, M. Montano, J. Goldberger, G. Somorjai and P. D. Yang, *Nano Lett.*, 2005, **5**, 1231–1236.
33 J. Rybczynski, D. Banerjee, A. Kosiorek, M. Giersig and Z. F. Ren, *Nano Lett.*, 2004, **4**, 2037–2040.
34 J. Rybczynski, U. Ebels and M. Giersig, *Colloids Surf., A*, 2003, **219**, 1–6.
35 M. Wang, S. H. Hahn, J. S. Kim, S. H. Hong, K.-K. Koo and E. J. Kim, *Mater. Lett.*, 2008, **62**, 4532–4534.
36 Z. Yang, Y.-Y. Shi, X.-L. Sun, H.-T. Cao, H.-M. Lu and X.-D. Liu, *Mater. Res. Bull.*, 2010, **45**, 474–480.
37 C. Li, G. J. Fang, J. Li, L. Ai, B. Z. Dong and X. Z. Zhao, *J. Phys. Chem. C*, 2008, **112**, 990–995.
38 Y. J. Kim, C. H. Lee, Y. J. Hong, G. C. Yi, S. S. Kim and H. Cheong, *Appl. Phys. Lett.*, 2006, **89**, 163128.
39 J. R. Duclere, R. O'Haire, A. Meaney, K. Johnston, I. Reid, G. Tobin, J. P. Mosnier, M. Guilloux-Viry, E. McGlynn and M. O. Henry, *J. Mater. Sci.: Mater. Electron.*, 2005, **16**, 421–427.
40 B. K. Meyer, H. Alves, D. M. Hofmann, W. Kriegseis, D. Forster, F. Bertram, J. Christen, A. Hoffmann, M. Strassburg, M. Dworzak, U. Haboeck and A. V. Rodina, *Phys. Status Solidi B*, 2004, **241**, 231–260.
41 M. Strassburg, A. Rodina, M. Dworzak, U. Haboeck, I. L. Krestnikov, A. Hoffmann, O. Gelhausen, M. R. Phillips, H. R. Alves, A. Zeuner, D. M. Hofmann and B. K. Meyer, *Phys. Status Solidi B*, 2004, **241**, 607–611.
42 M. Biswas, PhD thesis, Dublin City University, 2010.
43 K. Vanheusden, W. L. Warren, C. H. Seager, D. R. Tallant, J. A. Voigt and B. E. Gnade, *J. Appl. Phys.*, 1996, **79**, 7983–7990.
44 M. D. McCluskey and S. J. Jokela, *J. Appl. Phys.*, 2009, **106**, 071101.

